Molecular Therapy
Oncolytics
Original Article

Icaritin inhibits PLK1 to activate DNA damage response in NK/T cell lymphoma and increases sensitivity to GELOX regime

Canjing Zhang,[1,3,5] Huiwen Xu,[1,2,5] Xianxian Sui,[3] Lina Chen,[1] Bobin Chen,[2] Haozhen Lv,[4] Songmei Wang,[3] and Xuanyi Wang[1]

[1]Key Laboratory of Medical Molecular Virology of Ministry of Education & Ministry of Health, School of Basic Medical Sciences and Institutes of Biomedical Sciences, Fudan University, Shanghai 200032, People's Republic of China; [2]Department of Hematology, Huashan Hospital, Fudan University, Shanghai 200040, People's Republic of China; [3]Laboratory of Medical Molecular Biology, Experimental Teaching Center, School of Basic Medical Sciences, Fudan University, Shanghai 200032, People's Republic of China; [4]Shanghai Medical College, Fudan University, Shanghai 200032, People's Republic of China

Natural killer/T cell lymphoma (NKTCL) is a highly aggressive subtype of non-Hodgkin lymphoma. Gemcitabine, oxaliplatin, and L-asparaginase (GELOX) is one of the first-line chemotherapy regimens of NKTCL. Yet, the prognosis of NKTCL is poor. Icaritin is an herb-derived monomer from icariin with antitumor effects. We found that icaritin induced proliferation inhibition and apoptosis of NKTCL both *in vitro* and *in vivo*. Moreover, icaritin inhibited the dissemination of NKTCL *in vivo*. RNA sequencing revealed the Polo-like kinase 1 (PLK1) gene and DNA damage response (DDR) as the targets of icaritin. Mechanistically, icaritin inhibited PLK1 to promote checkpoint kinase 2 (Chk2) homodimerization and its T387 phosphorylation, which further activated p53, leading to the activation of the DDR pathway. Moreover, inhibiting PLK1 increased Forkhead box O3a nuclear localization, the latter of which activated ataxia telangiectasia mutated (ATM), an early sensor of DNA damage. Then ATM phosphorylated Chk2 T68 and initiated Chk2 activation. Remarkably, the combined treatment of icaritin and GELOX achieved better antitumor efficacy than single treatment *in vivo*. In summary, our results proved the efficacy of icaritin treating NKTCL, provided insights into its antitumor molecular mechanism, and revealed the application value of icaritin in facilitating clinical NKTCL treatment.

INTRODUCTION

Natural killer/T cell lymphoma (NKTCL) is an Epstein-Barr virus-associated non-Hodgkin lymphoma subtype originated from malignant proliferating NK cell or T cell lineage.[1] NKTCL commonly occurs in the upper aerodigestive tract, with more frequent occurrence in Asia and South American.[2] Owing to the resistance to anthracycline of NKTCL, non-anthracycline-regimens containing L-asparaginase are recommended as first-line therapy.[3] The dexamethasone, methotrexate, ifosfamide, L-asparaginase, and etoposide regimen achieves a 5-year overall survival (OS) rate of 47%–52%.[4] However, severe hematologic toxicity (42%–67%) and treatment-related mortality (5%–6%) hinder its clinical application and therapeutic effects.[4,5] Patients with stage III-IV NKTCL treated with the combined radiotherapy and GELOX regimen have a median OS of only 8.1 months.[6]

The pathogenesis of NKTCL has not been fully understood, but the deregulation of the DNA damage response (DDR) may play a role.[7] DNA lesions occur constantly owing to the assaults of endogenous metabolites and environmental stressors. In response to DNA double-strand breaks (DSBs), the immediate-early sensors ataxia telangiectasia mutated (ATM) activates and then phosphorylates checkpoint kinase 2 (Chk2) on its Thr68 site.[8] Once phosphorylated, the Thr68 segment of Chk2 binds to the forkhead-associated (FHA) domain of another Chk2 molecule, forming homo-dimers and promoting the phosphorylation of Thr383 and Thr387 in the T loop of the catalytic domain of Chk2.[9] ATM and Chk2 both can activate and stabilize p53, which induces the expression of genes involved in cell cycle checkpoint activation or apoptosis.[10] ATM also phosphorylates the Ser139 site of histone H2A variant, forming γH2Ax, to assemble DNA repair proteins and amplify the DDR signaling.[11] These DDR core molecules respond to DNA lesions, promoting DNA repair and cell survival or cell apoptosis. The decision between which depends on the DNA damage severity and the cell damage tolerance.[12] Eliminating cells with unrepaired damage by inducing apoptosis is an important tumor suppressor function of the DDR pathway.[13] The

Received 27 October 2021; accepted 29 April 2022;
https://doi.org/10.1016/j.omto.2022.04.012.

[5]These authors contributed equally

Correspondence: Songmei Wang, Laboratory of Medical Molecular Biology, Experimental Teaching Center, School of Basic Medical Sciences, Fudan University, Shanghai 200032, People's Republic of China.
E-mail: smwang2@fudan.edu.cn
Correspondence: Xuanyi Wang, Key Laboratory of Medical Molecular Virology of Ministry of Education & Ministry of Health, School of Basic Medical Sciences and Institutes of Biomedical Sciences, Fudan University, Shanghai 200032, People's Republic of China.
E-mail: xywang@shmu.edu.cn

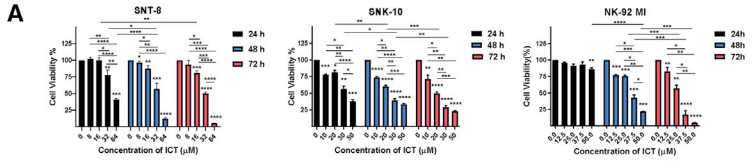

Cell/IC50(μM)	24h	48h
SNT-8	54.75	34.26
SNK-10	44.26	25.01
NK-92 MI	32.92	25.20

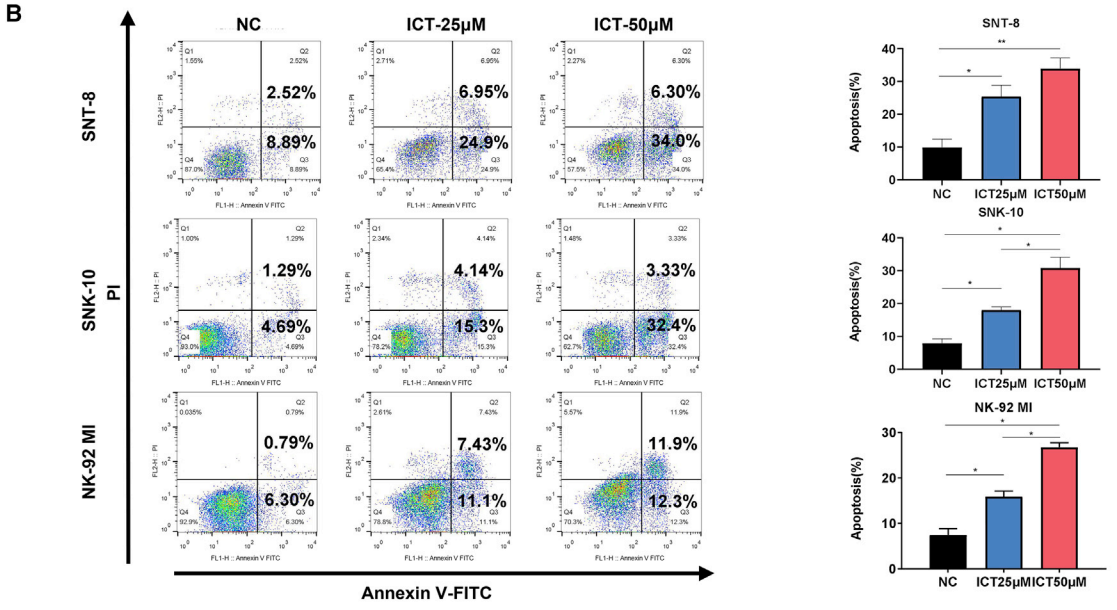

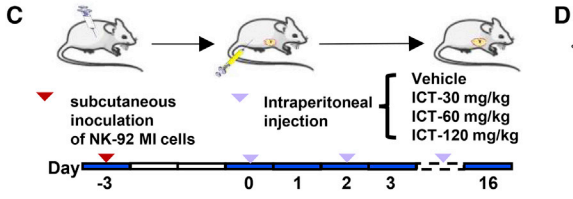

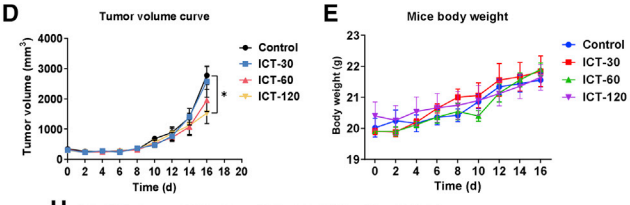

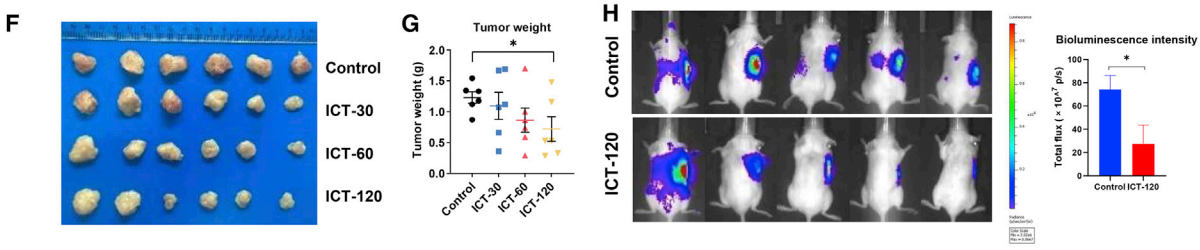

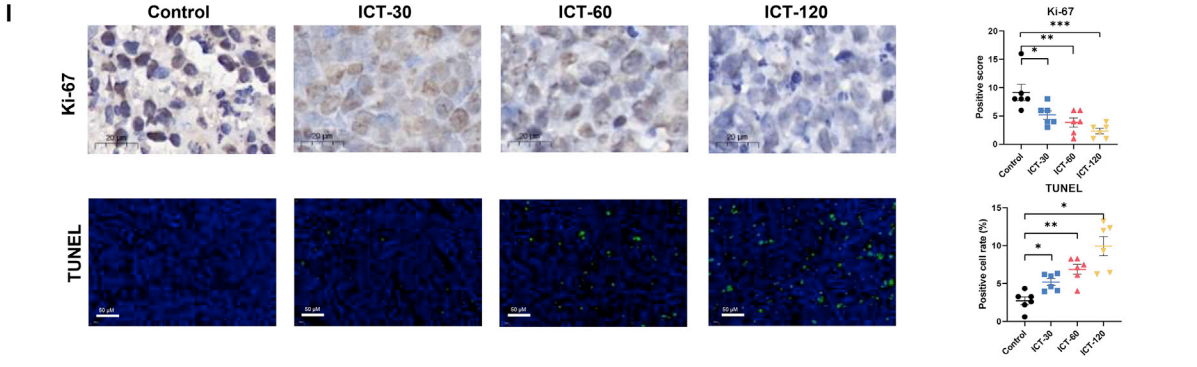

(legend on next page)

defective DDR accumulates genomic aberrations, which favors tumorigenesis and progression.[14] A DDR defect is commonly observed in cancers.[15,16] Our earlier work found that the DSBs sensor ATM was hyper-phosphorylated in NKTCL, while its downstream factors Chk2 and p53 were not, revealing the malfunctioning DDR pathway in NKTCL.[17]

A DDR defect is at least partly resulted from Polo-like kinase 1 (PLK1) overexpression in tumors.[18] PLK1 is a serine/threonine kinase expressed in dividing cells with peak expression during G2/M.[19] As a cell cycle regulator, it is essential for mitosis and DNA integrity maintenance.[20] PLK1 is closely related to the DDR pathway.[18,21] For example, PLK1 phosphorylates the FHA domain of Chk2 to prevent its dimerization and its recruitment to DSBs.[22,23] Moreover, PLK1 inhibits Forkhead box O3a (FOXO3a), a tumor suppressor that interacts with ATM and promotes its activation.[24,25]

Traditional Chinese medicine (TCM) shows great potential in cancer treatment.[26] Icaritin (ICT) derives from icariin, a flavonoid component extracted from plants of the *Epimedium* genus, with biological activities including neuroprotection,[27,28] suppression of osteoclast differentiation,[29] and the promotion of embryonic stem cells differentiating into cardiomyocytes.[30] It is also a potent and selective antitumor candidate drug proved in liver cancer, lung cancer, prostate cancer, breast cancer, colon cancer, bladder cancer, endometrial cancer, acute myeloid leukemia, and chronic myeloid leukemia, with low toxicity to normal cells and animals.[31–40] In the current study, we aimed to investigate its ability to inhibit NKTCL and the underlying mechanism.

Here, we found that ICT potently inhibited the proliferation and induced apoptosis of NKTCL *in vitro*, and inhibited its growth and dissemination *in vivo*. By inhibiting PLK1, ICT increased Chk2 homo-dimerization and activated p53. Inhibiting PLK1 also increased FOXO3a nuclear localization and further activated ATM, symbolizing the DDR pathway activation. Intriguingly, the combined application of ICT and the GELOX regimen achieved a better tumor suppression effect than that of the GELOX regimen alone in NKTCL xenografts.

RESULTS

ICT inhibits the growth and induces cell apoptosis of NKTCL both *in vitro* and *in vivo*

SNT-8, SNK-10, and NK-92 MI cells were treated with different concentrations of ICT for 24, 48, and 72 h. A CCK-8 assay revealed lower cell viability as the ICT concentration and treatment time increased (Figure 1A). The half maximal inhibitory concentration (IC_{50}) values of 24 hour-ICT treatment for SNT-8, SNK-10, and NK-92 MI cells were 54.75, 44.26, and 32.92 μM, respectively (Figure 1A). The IC_{50} values of 48-h ICT treatment for SNT-8, SNK-10, and NK-92 MI cells were 34.26, 25.01, and 25.20 μM, respectively (Figure 1A). ICT significantly inhibited cell proliferation in a dose- and time-dependent manner (Figure 1A). Cell count data confirmed the inhibitory effect of ICT on NKTCL cells, which showed that ICT decreased the NKTCL cell number dose dependently (Figure S1). Then we examined the apoptotic rates of three NKTCL cell lines treated with DMSO or 25 or 50 μM ICT for 48 h using annexin V/PI dual staining and flow cytometry assay. The apoptosis rates of untreated SNT-8, SNK-10, and NK-92 MI cells were 9.9%, 7.9%, and 7.5%, respectively (Figure 1B). After 48 h of treatment with 25 μM ICT, the average apoptosis rates of SNT-8, SNK-10, and NK-92MI cells increased to 25.3%, 18.0%, and 15.9%, respectively (Figure 1B). After 48 h of treatment with 50 μM ICT, the apoptosis rates of SNT-8, SNK-10, and NK-92MI cells increased to 33.9%, 30.8%, and 26.8%, respectively (Figure 1B). ICT induced apoptosis in three cell lines significantly. Moreover, 50 μM ICT induced a significantly higher apoptosis rate than 25 μM ICT in SNK-10 and NK-92 MI cells (Figure 1B). ICT induced apoptosis of the SNK-10 and NK-92 MI cell lines in a dose-dependent manner (Figure 1B). In contrast, ICT did not influence the apoptosis rates in normal human cells, including primary NK cells, human embryonic kidney cell line 293T, and human liver cell line QSG-7701 (Figures S2 and S3).

To investigate the *in vivo* efficacy of ICT treating NKTCL, a xenograft model developed using NK-92 MI cell line was used. The tumor-bearing mice were treated with dissolvent (control), 30 mg/kg, 60 mg/kg, or 120 mg/kg ICT (Figure 1C). Notably, the tumor growth was significantly suppressed by 120 mg/kg ICT, compared with those in control group, as shown by the tumor volume curve (Figure 1D). During the whole treatment period, the mice weight of the 30, 60, and 120 mg/kg ICT groups showed no difference from that of control group (Figure 1E). At the end of treatment, tumor tissues were collected and weighed (Figure 1F). The weight of the tumors in the ICT group was lighter than those in the control group (Figure 1G). To evaluate the effect of ICT on the dissemination of NKTCL, we established a mouse model using NK-92 MI cells stably transfected with luciferase gene (NK-92 MI Luc). After being treated with 120 mg/kg ICT or vehicle for 16 days, only one in five mice of the ICT group had

Figure 1. ICT inhibits NKTCL growth *in vitro* and *in vivo*

(A) ICT inhibited the viability of NKTCL cells. SNT-8, SNK10 and NK-92 MI cells were treated with the indicated concentrations of ICT for 24, 48, and 72 h. Cell viability was measured by CCK-8 assay (left). Data are presented as mean ± standard error of the mean (n = 3). The IC50 of NKTCL cells treated with ICT for 24 and 48 h were calculated (right). (B) ICT induced apoptosis of NKTCL cell lines. NKTCL cells were treated with 0, 25, and 50 μM ICT for 48 h and the apoptosis was measured by Annexin V-FITC/PI double staining and flow cytometry. Representative results were shown and percentage of apoptotic cells was plotted. Data were represented as mean ± standard error of the mean (n = 3). (C) The mice were inoculated with NK-92 MI cells subcutaneously and randomized into four groups (n = 6/group). Tumor inoculation and treatment scheme were shown. (D) Tumor volumes measured at the indicated time. (E) Mice body weight measured at the indicated time. (F) The photo of isolated tumors derived from mice treated with vehicle or 30, 60, or 120 mg/kg ICT. (G) Tumor weights measured after mice sacrifice. (H) Bioluminescence imaging of NK-92 MI LUC-tumor bearing mice in control and ICT 120 mg/kg groups (n = 5/group). (I) The Ki67 expression in tumor xenografts was examined by IHC. The apoptosis rate was assessed by TUNEL assay. Nuclei were stained with DAPI (blue). Green points indicate the TUNEL-positive nuclei. Representative images were shown. *p < 0.05; **p < 0.01; ***p < 0.001; ****p < 0.0001. Scale bar, 20 μm or 50 μm.

distant dissemination of NKTCL in the whole body, compared with four in five mice in the control group, showing the profound inhibition by ICT to NKTCL xenograft dissemination (Figure 1H). Tumor tissues in the ICT groups gained significantly lower positive scores of Ki-67, which is a marker of proliferation, than in the control group (Figure 1I). The terminal deoxynucleotidyl transferase (TUNEL) assay revealed a notably higher apoptotic cell rate of ICT-treated tumors, compared with the control group (Figure 1H). Taken together, ICT suppresses NKTCL growth and induces apoptosis both *in vitro* and *in vivo*.

RNA-sequencing data reveals that ICT inhibits PLK1 and activates DDR and FOXO pathway in NKTCL

To decipher the underlying mechanisms of ICT inhibiting growth and inducing apoptosis of NKTCL, we conducted RNA-sequencing (RNA-seq) of three NKTCL cell lines treated with or without ICT. After standardization of the RNA sequence results, differentially expressed genes (DEGs) were identified (185 up and 180 down in SNT-8 cells, 179 up and 241 down in SNK-10 cells, and 167 up and 156 down in SNT-16 cells) (Figure 2A). The overlap among the three DEG sets contained 110 genes (Figure 2B). Normal human cell lines 293T and QSG-7701 were used to test the safety of ICT. The RNA-seq results of 293T and QSG-7701 cells revealed only three and eight DEGs regulated by ICT, respectively (Tables S1 and S2).

The biological functions of the DEGs in SNT-8, SNK-10 and NK-92 MI cells were analyzed using the Database for Annotation, Visualization and Integrated Discovery (DAVID). The gene ontology (GO) analysis results showed that DEGs were significantly enriched in biological processes (BP), including cell proliferation, apoptotic process, DDR, cell cycle regulation, cell division, negative regulation of transcription from RNA polymerase II promoter, immune response, response to endoplasmic reticulum stress, and cellular response to hypoxia, and so on (Table 1). Among the DEGs involved in the top 20 BP regulated by ICT, the PLK1 gene was related to 7 of 20 processes, including the negative regulation of transcription from RNA polymerase II promoter, regulation of the cell cycle, cell proliferation, mitotic nuclear division, protein ubiquitination involved in ubiquitin-dependent protein catabolic process, anaphase-promoting complex-dependent catabolic process, and G2/M transition of the mitotic cell cycle (Table 1). The Kyoto Encyclopedia of Genes and Genomes (KEGG) pathway analysis revealed that DEGs were enriched in p53, FOXO, cell cycle, cytokine-cytokine receptor interaction, and the mitogen-activated protein kinase signaling pathway (Figure 2C). The DEGs involved in the p53, FOXO, and apoptosis pathways were shown by a heatmap (Figure 2D). PLK1 was involved in the FOXO pathway (Figure 2D). To better understand the interaction between the DEGs, the PPI network of DEGs was constructed using Cytoscape, with 64 nodes and 174 edges (Figure 2E). The possible initiative genes which were closely interacting with other genes were acquired by conducting a molecular complex detection (MCODE) analysis. One core module was amplified as shown by the red arrow (Figure 2E). PLK1, as one of the hub genes, the mRNA expression was drastically reduced by ICT in three NKTCL cell lines (Figure 2F). To verify the role of PLK1 in NKTCL tumorigenesis, we collected the PLK1 mRNA expression data of normal lymph nodes and NKTCL cell lines from the GEO databases GSE63548, GSE25297, GSE36172, and GSE19067. The PLK1 expression in NKTCL cell lines was significantly higher than that in normal lymph nodes (Figure 2G). Collectively, the RNA-seq results indicated that ICT regulated the p53 and FOXO pathway, and DDR in NKTCL cells. Among all the DEGs regulated by ICT, PLK1 was a core gene involved in the proliferation and apoptosis processes and the FOXO pathway.

ICT induces NKTCL cell apoptosis by decreasing PLK1 expression

Because the RNA-seq results predicted that PLK1 was a possible core gene in the antitumor mechanism of ICT, we detected the mRNA and protein levels of PLK1 in NKTCL cell lines treated with ICT. In accordance with the RNA-seq results, the mRNA level of PLK1 was decreased by ICT in three NKTCL cell lines (Figure 3A). Further, the total and phosphorylation levels of PLK1 protein were also decreased by ICT (Figure 3B). Quantitative analyses of the protein levels of p-PLK1 and PLK1 are shown (Figures 3C and 3D). To determine the role of PLK1 inhibition in ICT-induced proliferation inhibition and apoptosis, we constructed the tetracycline-inducible (tet on) PLK1 overexpression and the empty vector (EV) NK-92 MI cells. To test the PLK1 overexpression efficiency, doxycycline (DOX) was used to treat the tet on PLK1 cells or EV cells. The mRNA expression of PLK1 drastically increased after 12 h or 24 h treatment of 2 μg/mL or 4 μg/mL DOX (Figure 3E). The protein level of PLK1 also improved after 2 μg/mL DOX treatment for 24 h (Figure 3F). These results indicated the successful induction of PLK1 expression by DOX. To know whether overexpressing PLK1 in ICT-treated NKTCL cells could rescue ICT-induced cell apoptosis, we examined the apoptosis rate of tet on PLK1 and EV cells after being treated by ICT for 24 h followed with or without DOX treatment. The DOX treatment attenuated apoptosis in tet on PLK1 cells but not in EV cells, indicating the importance of PLK1 to cell survival (Figure 3G). To further prove the role of PLK1 in ICT-induced proliferation inhibition and apoptosis, a PLK1 inhibitor BI 2536 was used. BI 2536 inhibited the proliferation of SNT-8, SNK-10, and NK-92 MI cells dose dependently (Figure 3H). Also, BI 2536 induced apoptosis in three NKTCL cell lines (Figure 3I). These results suggested that PLK1 was crucial for ICT to inhibit cell proliferation and induce apoptosis in NKTCL.

PLK1 interacts with Chk2 to activate the DDR pathway

PLK1 was reported to inhibit Chk2, a core molecule of DDR pathway, by hindering Chk2 homo-dimerization.[22,41] Also, as predicted by the RNA-seq results, ICT activated the DDR pathway in NKTCL. Thus, we investigated whether Chk2 was regulated by ICT. First, we detected the Chk2 dimer in ICT-treated NKTCL cells by performing intracellular cross-linking using DSS. The dimerization of Chk2 and its Thr387 phosphorylation in SNT-8, SNK-10, and NK-92 MI cells increased by ICT treatment over time (Figure 4A). The grayscale analyses of the protein bands of Chk2 dimer, monomer, and T387 phosphorylation were conducted (Figure S4). In SNT-8 cells, ICT

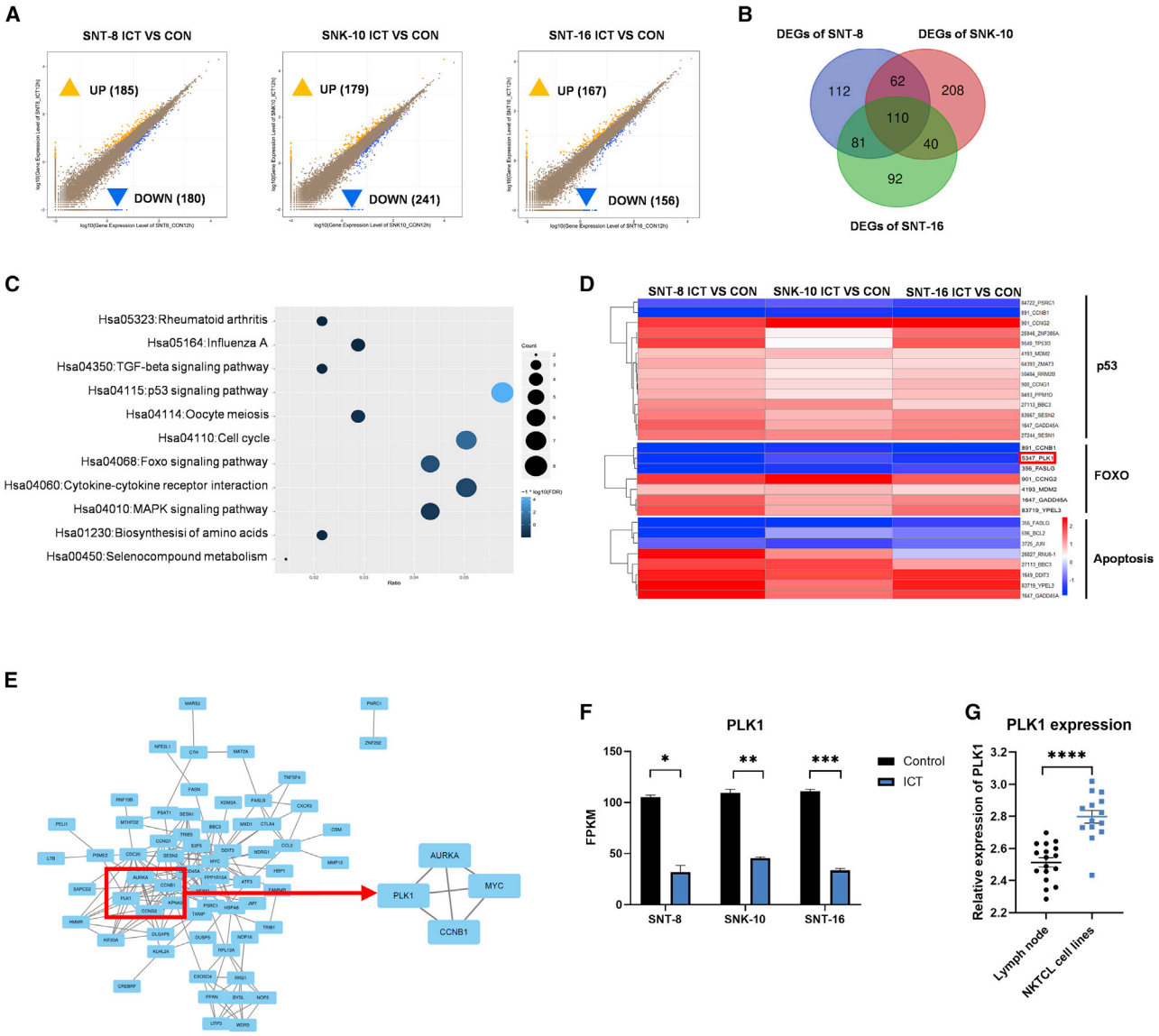

Figure 2. Bioinformatic analysis reveals that ICT down-regulates PLK1 and activates the apoptosis, p53 and FOXO pathway

(A) DEGs of SNT-8, SNK-10, and NK-92 MI cell lines treated with DMSO or ICT were selected with a fold change of 2 or greater and a p value of less than 0.05. Orange for up-regulated genes and blue for down-regulated genes. (B) The Venn diagram showed the overlap of 110 genes among 3 datasets. (C) The bubble plot showed the KEGG results of the 110 genes. (D) Heatmap of genes enriched in p53, FOXO and apoptosis signaling pathways. (E) The PPI network of 110 enriched genes was constructed using Cytoscape. One of the core modules of DEGs obtained by MCODE from PPI network was shown by red arrow. (F) The FPKM value of PLK1 gene in three NKTCL cell lines treated with DMSO or ICT were shown. (G) The expression of PLK1 in normal lymph nodes and NKTCL cell lines. The data were acquired from the GSE63548, GSE25297, GSE36172, and GSE19067 datasets of the GEO database. *p < 0.05; **p < 0.01; ***p < 0.001; ****p < 0.0001.

increased the Chk2 dimer and monomer significantly after 12 and 24 h of treatment, and increased its T387 phosphorylation in 3-48 h (Figure 4A). In SNK-10 cells, ICT increased the Chk2 dimer continuously in 6-48 h, and increased its monomer form and T387 phosphorylation in 3-48 h (Figure 4A). The dimerization of Chk2 and its Thr387 phosphorylation in NK-92 MI cells increased transiently and potently after ICT treatment for 3 h (Figure 4A). The monomer form of Chk2 in NK-92 MI cells increased after ICT treatment for 6 h and maintained at a high level within 48 h (Figure 4A). The downstream factor of Chk2, p53, was also activated by ICT (Figure 4A). Further, the co-immunoprecipitation (Co-IP) assay showed that Chk2 coimmunoprecipitated with PLK1 and vice versa, revealing the physical interaction between PLK1 and Chk2 (Figures 4B and 4C).

Next, we tried to figure out whether ICT regulates Chk2 through PLK1. The tet on PLK1 and EV cells were treated with ICT for 12

Table 1. The top 20 BP regulated by ICT

Term	Count	p Value	Genes
GO:0000122~negative regulation of transcription from RNA polymerase II promoter	13	2.34E-04	**PLK1**, FASLG, KLF16, SFPQ, MYC, DDIT3, MDM2, CREBRF, TXNIP, TRIB3, MXD1, ATF3, HIST1H1C
GO:0008284~positive regulation of cell proliferation	10	5.27E-04	CDC20, CCPG1, MYC, CXCR3, TNFSF4, NOP2, OSM, MDM2, FASLG, ATF3
GO:0045944~positive regulation of transcription from RNA polymerase II promoter	10	0.056048	KDM3A, CCPG1, MYC, CXCR3, DDIT3, ZNF292, OSM, E2F5, ATF3, NFE2L1
GO:0051726~regulation of cell cycle	7	3.65E-05	HSPA8, CCNB1, GADD45A, CCNG2, **PLK1**, CCNG1, E2F5
GO:0008283~cell proliferation	7	0.010058	MYC, **PLK1**, OSM, POLR3G, MXD1, DLGAP5, BYSL
GO:0006955~immune response	7	0.018886	RGS1, TNFSF4, OSM, CTLA4, CCL2, FASLG, LTB
GO:0032436~positive regulation of proteasomal ubiquitin-dependent protein catabolic process	6	1.68E-05	PLK1, MDM2, RNF19B, TRIB3, TRIB1, AURKA
GO:0007050~cell cycle arrest	6	7.05E-04	PPP1R15A, GADD45A, MYC, DDIT3, JMY, HBP1
GO:0042787~protein ubiquitination involved in ubiquitin-dependent protein catabolic process	6	0.001018	CDC20, CCNB1, **PLK1**, MDM2, RNF19B, AURKA
GO:0043065~positive regulation of apoptotic process	6	0.017274	BNIP3L, GADD45A, JMY, TXNIP, CTLA4, FASLG
GO:0051301~cell division	6	0.030981	CDC20, CCNB1, PSRC1, CCNG2, CCNG1, AURKA
GO:0034976~response to endoplasmic reticulum stress	5	5.41E-04	PPP1R15A, DDIT3, CREBRF, TRIB3, BBC3
GO:0071456~cellular response to hypoxia	5	0.001365	BNIP3L, CCNB1, MDM2, NDRG1, BBC3
GO:0006974~cellular response to DNA damage stimulus	5	0.020447	PPP1R15A, MYC, DDIT3, CTLA4, BBC3
GO:0042981~regulation of apoptotic process	5	0.022086	BNIP3L, SDF2L1, NDRG1, INHBE, BBC3
GO:0007067~mitotic nuclear division	5	0.035793	CDC20, CCNG2, **PLK1**, CCNG1, AURKA
GO:0070059~intrinsic apoptotic signaling pathway in response to endoplasmic reticulum stress	4	5.91E-04	PPP1R15A, DDIT3, TRIB3, BBC3
GO:0006977~DDR, signal transduction by p53 class mediator resulting in cell cycle arrest	4	0.003692	CCNB1, GADD45A, MDM2, AURKA
GO:0031145~anaphase-promoting complex-dependent catabolic process	4	0.007265	CDC20, CCNB1, **PLK1**, AURKA
GO:0000086~G2/M transition of mitotic cell cycle	4	0.031355	CCNB1, **PLK1**, HMMR, AURKA

h, followed with or without DOX treatment for 12 h. Consistently, the inhibited PLK1 by ICT was recovered by DOX in tet on PLK1 NK-92 MI cells (Figure 4D). As a result, the ICT-induced Chk2 dimerization was also attenuated (Figure 4D). To further confirm the Chk2 regulation function of PLK1, we treated the three NKTCL cell lines with PLK1 inhibitor BI 2536 and detected the Chk2 level. Just like ICT, BI 2536 inhibited PLK1, while it increased Chk2 dimerization and p53 phosphorylation (Figure 4E). Taken together, ICT activated Chk2 by inhibiting PLK1, thus activating the DDR pathway in NKTCL.

PLK1 promotes FOXO3a nuclear localization to activate the DDR pathway

FOXO3a is a transcription factor concerning cell fate and has close interaction with the DDR pathway.[42] It exerts function in nuclear or mitochondria while losing activity in cytoplasmic.[43] Revealed by the RNA-seq result, ICT regulated FOXO pathway in NKTCL. ICT increased the nuclear localization of FOXO3a while leaving cytoplasmic FOXO3a unchanged or decreased in three NKTCL cell lines (Figure 5A). Moreover, ICT activated the early sensor of DNA damage, ATM. ATM then phosphorylated Chk2 at the T68 site (Figure 5A). The DNA damage marker protein γH2Ax was also activated by ICT (Figure 5A).

Our RNA-seq results revealed that PLK1 was involved in the FOXO pathway. Confirmed by the Co-IP assay, PLK1 coimmunoprecipitated with FOXO3a and vice versa, indicating that PLK1 interacted with FOXO3a physically (Figures 5B and 5C). To test whether PLK1 regulates FOXO3a, we used the tet on PLK1 NK-92 MI cells to achieve DOX-inducible PLK1 overexpression. We treat the tet on PLK1 and EV cells with ICT for 12 h to increase the FOXO3a nuclear localization. Then the subsequent 12-h DOX treatment decreased nuclear FOXO3a in tet on PLK1 cells (Figure 5D). Moreover, DOX reversed the ATM activation and Chk2 T68 phosphorylation by ICT (Figure 5D). In contrast, inhibiting PLK1 with its inhibitor BI 2536 increased nuclear FOXO3a and activated ATM and Chk2 T68 in NKTCL cells (Figure 5E). Consistently, immunofluorescence (IF) staining confirmed the distribution changes of FOXO3a. In untreated NK-92 MI cells, FOXO3a was mainly in the cytoplasm (Figure 5F). Both ICT and BI 2536 increased the FOXO3a nuclear

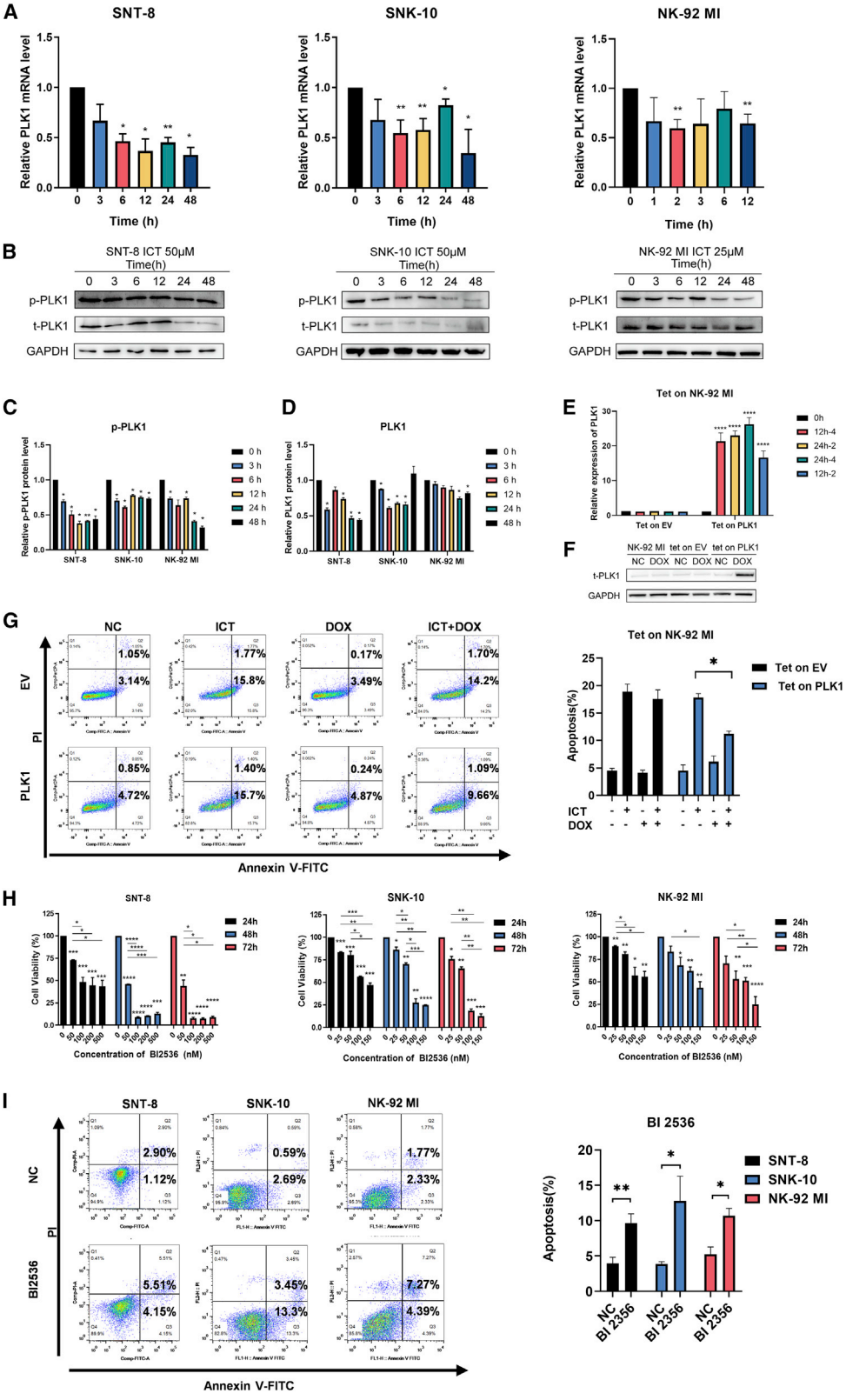

(legend on next page)

localization in NKTCL cells (Figure 5F). IF staining showed the colocalization of FOXO3a and PLK1 after ICT treatment (Figure 5G). These results indicated that by inhibiting PLK1, ICT promoted FOXO3a function to activate ATM and its downstream factor Chk2.

ICT inhibits PLK1 and activates the DDR pathway *in vivo*

To test the effects of ICT on PLK1 and DDR pathway *in vivo*, we collected the xenografts in four mice groups treated with resolvent, and 30, 60, or 120 mg/kg ICT and performed immunohistochemical (IHC) staining to detect PLK1 and the key molecules of the DDR pathway. Consistent with the *in vitro* experiment results, ICT-treated xenografts showed weaker staining intensity of PLK1 and stronger staining intensity of p-Chk2 T68 and p-p53 than those of the control group (Figure 6A). Moreover, ICT exerted no influence on the PLK1 expression in healthy mice organs, including the liver, kidney, and spleen (Figure S5). Western blot results of xenograft tissue extracts revealed the decreased p-PLK1 and elevated p-ATM, p-Chk2 T68, p-p53, and γH2Ax in 120 mg/kg of the ICT group compared with those in the control group (Figure 6B). The grayscale analyses further verified the western blot results (Figure 6B).

ICT enhances the treatment effect of the GELOX regimen *in vivo*

The GELOX regimen is currently the first-line chemotherapy of NKTCL. To determine whether ICT could facilitate clinical therapy, we applied the GELOX regimen and/or 120 mg/kg of ICT treatment in NKTCL mouse model (Figure 7A). Both the GELOX regimen and ICT showed tumor growth inhibition effect (Figure 7B). The combination of them showed improved inhibition effects on tumor growth (Figure 7B). The xenografts were collected and weighed after treatment finished. The xenografts of the combined treatment group were significantly smaller and lighter than that of the ICT or GELOX group (Figures 7C and 7D). Moreover, the body weight of mice treated with ICT and/or GELOX regime showed no difference with those in the control group during the treatment period, indicating that the combination of ICT and GELOX regimen did not cause toxic side effects to mice (Figure 7E). The combination treatment of ICT and GELOX significantly inhibited tumor proliferation as showed by the Ki-67 staining, and increased the apoptosis rate shown by the TUNEL results of xenografts (Figure 7F). These results highlighted that ICT facilitated the treatment effect of the GELOX regimen.

DISCUSSION

TCM has potential in tumor treatment for promising antitumor activity and the ability to facilitate chemotherapy efficacy and ameliorate drug resistance.[44] As a monomer agent extracted from *Epimedium*, ICT was first found the ability to inhibit NKTCL *in vitro* in our previous work in 2015.[45] Here, we further proved the *in vivo* antitumor effects of ICT on NKTCL. We also demonstrated the molecular mechanisms comprehensively by performing RNA-seq and verified PLK1 inhibition and DDR activation function of ICT for the first time. An inspiring result was that ICT facilitated the antitumor efficacy of the GELOX regimen *in vivo*. Our work enriched the studies of antitumor TCM and provided a new strategy for NKTCL treatment.

Tens of thousands of DNA lesions accumulate constantly in each cell every day.[46] DDR is a critical barrier combating the driver aberrations, genomic instability, and cell malignant transformation.[11] However, DDR is defective in various kinds of tumors, including NKTCL, making it an important antitumor target.[7] Consistently, a previous study of our team found that part of the DDR pathway was hindered midway in NKTCL tissues, with ATM overactivated while its downstream factors Chk2 and p53 unactivated, compared with the normal tissues.[17] The DDR defect also creates vulnerabilities in tumors and has been exploited as a target of antitumor therapy. On one hand, inducing excessive DNA damage beyond the repair capacity threshold of tumor cells has been the mainstream chemotherapy and radiotherapy strategy.[47] On the other hand, reactivating the defective DDR pathway in tumors is also a promising strategy.[48] NKTCL cells harbor more genome aberrations than normal cells, leaving a therapeutic window for DDR induction therapy.[49] If the defective DDR pathway is re-established, tumor cells will be more susceptible to DDR-induced apoptosis than normal cells. Our work found that ICT released the inhibition of the DDR pathway, leading to NKTCL cell apoptosis.

Interestingly, some researchers hold the perspective that inhibiting the DDR pathway in tumors can facilitate chemotherapy efficacy.[50,51] The inhibitors of DDR also have antitumor effects, just like the activators of DDR.[52] Because the DDR pathway in tumor cells is partly malfunctioning, DDR inhibitors that target on the remaining functional DDR molecules can kill the tumor cells.[53] Normal cells may survive relying on the other part of the DDR pathway function that

Figure 3. ICT inhibits cell proliferation and induces apoptosis by inhibiting PLK1

(A) SNT-8 and SNK-10 cells were treated with 50 μM of ICT for 0, 3, 6, 12, 24, and 48 h. NK-92 MI cells were treated with 25 μM of ICT for 0, 1, 2, 3, 6, and 12 h. The PLK1 mRNA expression was detected by qPCR. β-Actin was used as an internal reference. Data were presented as mean ± standard error of the mean (n = 3). (B) The protein levels of PLK1 and p-PLK1 in SNT-8, SNK-10, and NK-92 MI cells treated with ICT for the indicated time points were assessed by Western blot. GAPDH was used as a loading control. (C and D) The quantitative analyses of p-PLK1 and PLK1 protein levels in SNT-8, SNK-10, and NK-92 MI cells treated with ICT. (E) NK-92 MI cells stably transfected with tet on PLK1 or EV were treated with 2 or 4 mg/mL of DOX for 12 or 24 h. The mRNA level of PLK1 was detected by qPCR. (F) NK-92 MI, tet on PLK1 and EV cells were treated with 2 mg/mL of DOX for 24 h and the PLK1 protein level was detected using western blot. (G) NK-92 MI cells stably transfected with tet on PLK1 or EV were treated with 2 mg/mL DOX for 12 h, or 25 μM ICT for 24 h, or ICT for 24 h followed with DOX for 12 h. The apoptotic cell ratio was measured by Annexin V-FITC/PI double staining and flow cytometry. Representative images were shown. (H) SNT-8, SNK10, and NK-92 MI cells were treated with the indicated concentrations of BI 2536 for 24, 48 or 72 h. Cell viability was measured by CCK-8 assay. (I) The apoptotic cell ratio was measured after NKTCL cells were treated with BI 2536, ICT, or DMSO for 48 h. Representative images were shown. Data were presented as mean ± standard error of the mean (n = 3). *$p < 0.05$; **$p < 0.01$; ***$p < 0.001$; ****$p < 0.0001$. Tet on PLK1, tetracycline-inducible PLK1 overexpression NK-92 MI cells.

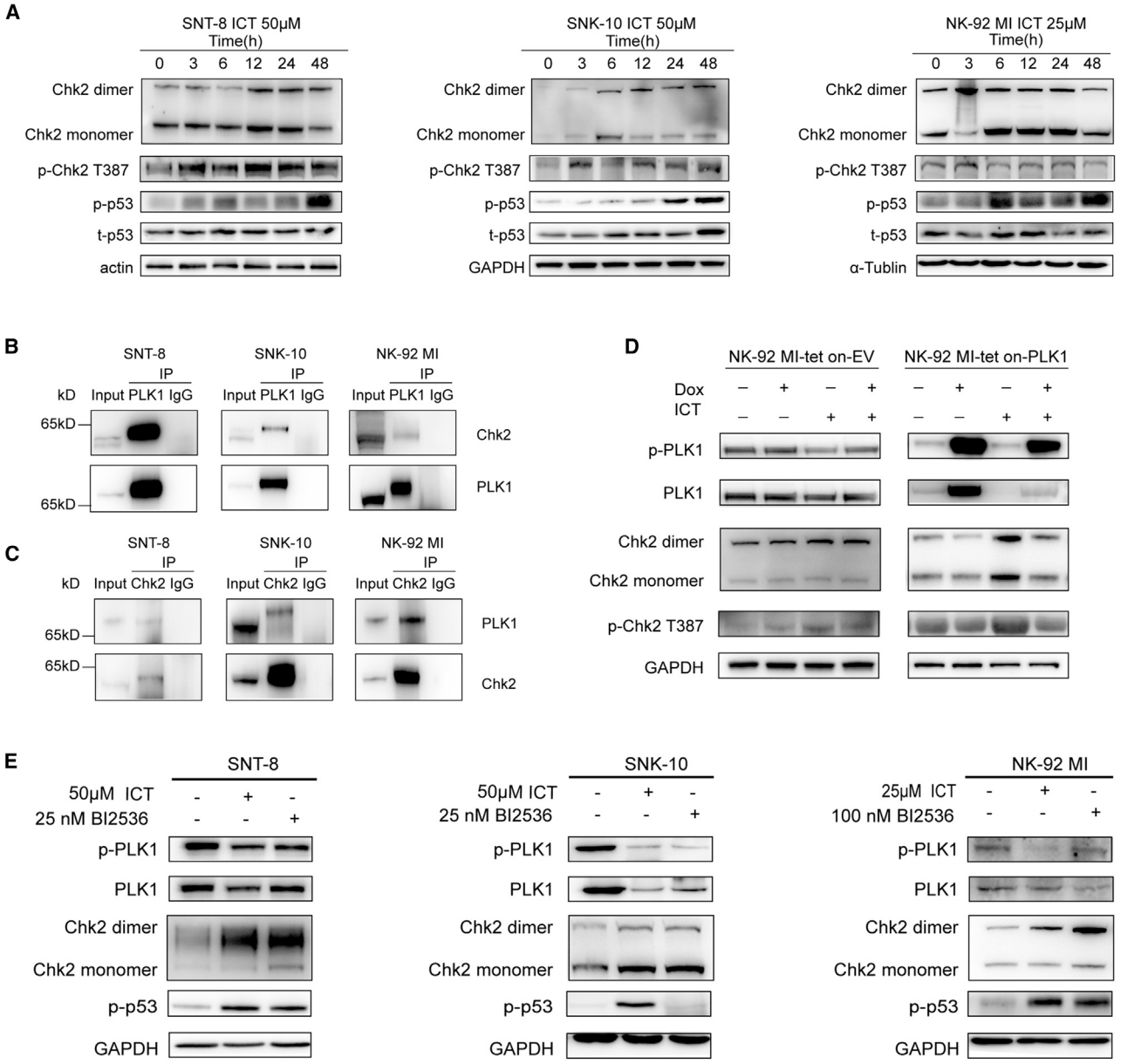

Figure 4. ICT promotes Chk2 dimerization and activation through inhibiting PLK1

(A) SNT-8 and SNK-10 cells were treated with 50 μM of ICT and NK-92 MI cells were treated with 25 μM of ICT for 0, 3, 6, 12, 24, or 48 h. Cell lysates were subjected to western blot to detect the indicated proteins (intracellular crosslinking using DSS was needed to detect Chk2 dimer). β-Actin, GAPDH, and α-tublin were used as loading controls. (B and C) Co-IP assay was performed using SNT-8, SNK-10, and NK-92 MI cells lysates. (B) The immune complexes were formed by pre-incubation with anti-PLK1 (IP PLK1) and revealed with Chk2 antibody or PLK1 antibody. (C) The immune complexes were formed by pre-incubation with anti-Chk2 (IP Chk2) and revealed with PLK1 antibody or Chk2 antibody. (D) Tet on PLK1 and EV cells were treated with DMSO, 2 mg/mL DOX for 12 h, 25 μM ICT for 12 h, or ICT for 12 h followed with DOX for 12 h. Western blot assay was conducted using indicated antibodies (intracellular crosslinking before cell lysis was performed to detect Chk2 dimer). GAPDH was used as a loading control. (E) SNT-8, SNK-10, and NK-92 MI cells were treated with ICT or BI 2536 and the indicated proteins were detected using western blot. GAPDH was used as a loading control. IP, immunoprecipitation; Tet on EV, tetracycline-inducible EV NK-92 MI cell line; Tet on PLK1, tetracycline-inducible PLK1 overexpression NK-92 MI cell line.

tumor cells lose during tumorigenesis.[11] Nonetheless, the defected part of DDR can alter to a great extent when it comes to different types of tumors.[11] Given that few mechanisms of the DDR defect elucidate when it comes to specific tumors, it is risky to use a common DDR inhibitor for all. Severe side effects might happen if essential molecules for normal cells but not tumor cells are targeted. Moreover,

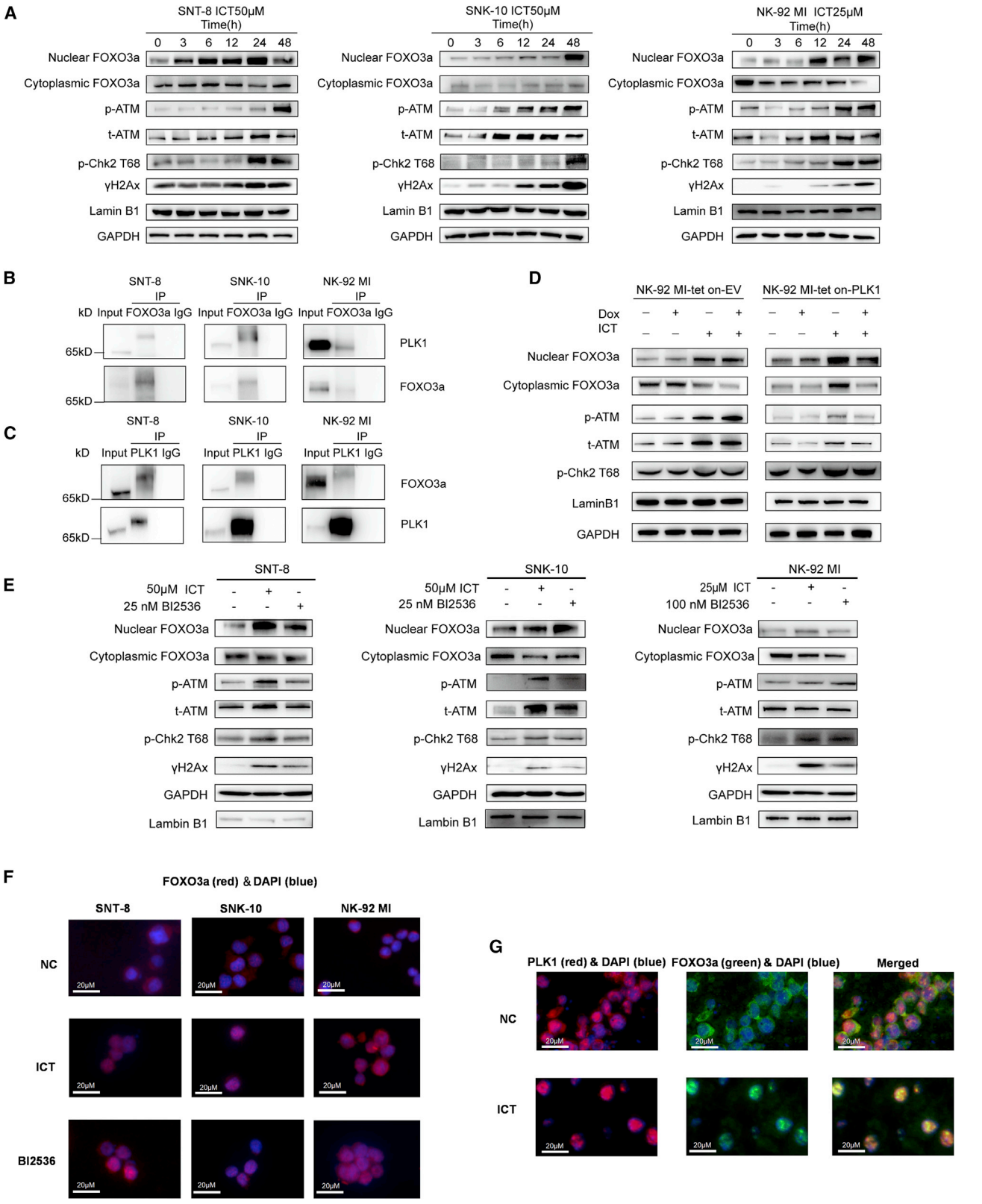

(legend on next page)

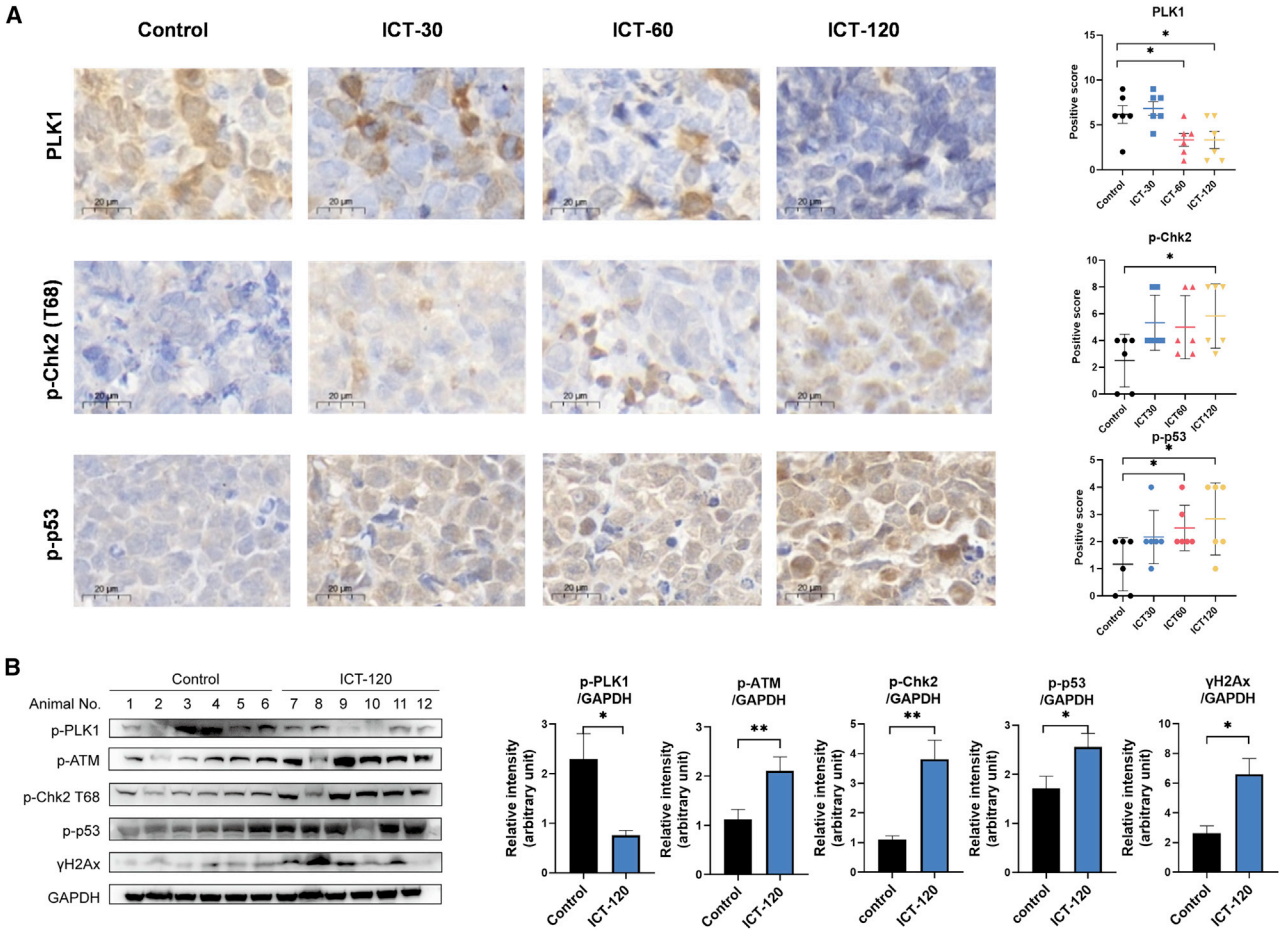

Figure 6. ICT inhibits PLK1 and activates DDR pathway *in vivo*

(A) Representative IHC images of tumor tissues from control, 30, 60, and 120 mg/kg of ICT mice group (left) and the quantification of IHC results (right). (B) Tumor tissue extracts (120 mg/kg of ICT group and control group) were subjected to western blot using the indicated antibodies (n = 6/group). GAPDH was used as a loading control (left). (Right) Densitometric analysis of the western blot. *$p < 0.05$; **$p < 0.01$. Scale bar, 20 μm.

current inhibitors of DDR have been reported to lack sufficient selectivity and a narrow therapeutic window, causing hematologic toxicities and off-target cardiotoxicity issues.[51] Our work focuses on targeting the DDR pathway in NKTCL. We believe that, by finding the specific driver factor that causes the DDR interruption in NKTCL and re-activating DDR, the regained DDR function will induce cell apoptosis, the destined fate of NKTCL cells that harbor too many genome errors. That is the reason we propose ICT as an antitumor drug and a chemosensitizer.

PLK1 has close interaction with the DDR pathway. Inhibiting PLK1 activates DDR and induces cell-cycle arrest, proliferation inhibition,

Figure 5. ICT promotes FOXO3a nuclear localization to activate ATM through inhibiting PLK1

(A) SNT-8 and SNK-10 cells were treated with 50 μM of ICT and NK-92 MI cells were treated with 25 μM of ICT for 0, 3, 6, 12, 24, or 48 h. Total cell lysates, cytoplasmic, and nuclear extracts were immunoblotted for the indicated proteins. GAPDH was used as a loading control. (B and C) Co-IP assay was performed using SNT-8, SNK-10, and NK-92 MI cells lysates. (B) The immune complexes were formed by pre-incubation with anti-PLK1 (IP PLK1) and revealed with FOXO3a antibody and PLK1 antibody. (C) The immune complexes were formed by pre-incubation with anti-FOXO3a (IP FOXO3a) and revealed with PLK1 antibody and FOXO3a antibody. (D) Tet on PLK1 and EV cells were treated with DMSO, 2 mg/mL DOX for 12 h, 25 μM ICT for 12 h, or ICT for 12 h followed by DOX for 12 h. The total cell lysates, cytoplasmic and nuclear extracts were subjected to the immunoblotting of indicated proteins. GAPDH was used as a loading control. (E) SNT-8, SNK-10, and NK-92 MI cells were treated with DMSO, ICT or BI 2536. The total cell lysates, cytoplasmic and nuclear extracts were subjected to the immunoblotting of indicated proteins. (F) Representative IF images of FOXO3a (red) in cells treated with DMSO, ICT, or BI 2536 for 48 h. Nuclei were stained with DAPI (blue). Three experiments were performed with similar results. (G) Double fluorescent immunostaining of PLK1 (red) and FOXO3a (green) of the xenograft tissues from the control group and the 120 mg/kg of ICT group. Nuclei were stained with DAPI (blue). Three experiments were performed with similar results. Scale bar, 20 μm. IP, immunoprecipitation; Tet on EV, tetracycline-inducible EV NK-92 MI cell line; Tet on PLK1, tetracycline-inducible PLK1 overexpression NK-92 MI cell line.

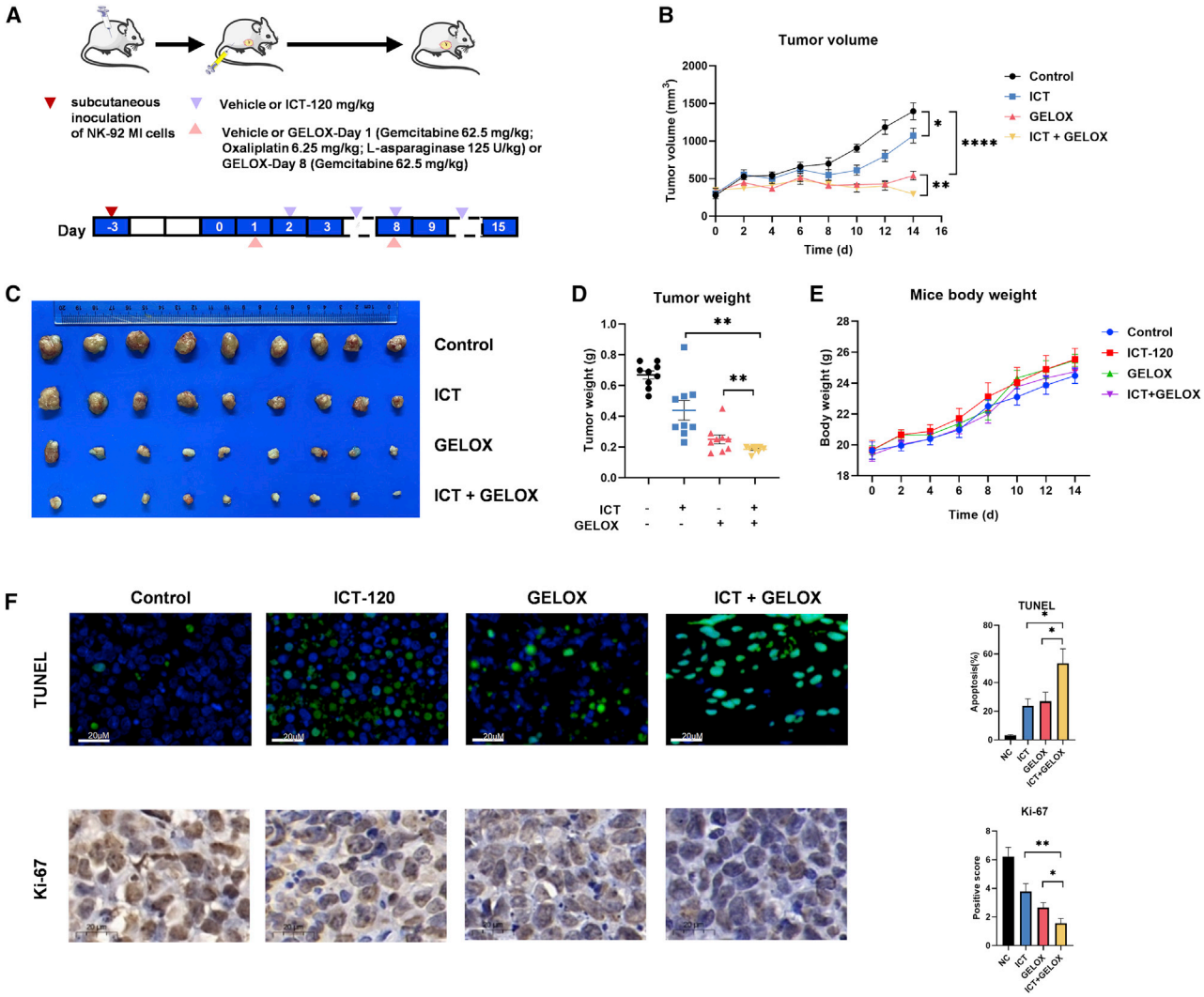

Figure 7. ICT facilitates GELOX regime *in vivo*

(A) The xenograft mice were treated with vehicle, ICT (120 mg/kg every other day) or/and GELOX regime (62.5 mg/kg gemcitabine, 6.25 mg/kg oxaliplatin, and 125 U/kg L-asparaginase at day 1, and 62.5 mg/kg gemcitabine at day 8). (B) Tumor volumes measured at the indicated time. (C) The photo of isolated xenografts. (D) Tumor weights after isolation. (E) Mice body weight measured at the indicated time. (F) Tumor xenograft sections of control, 120 mg/kg ICT, GELOX, and combined treatment of ICT and GELOX groups were examined by IHC analyses of Ki-67, and TUNEL assay. Nuclei were stained with DAPI (blue). Green points indicate the TUNEL-positive nuclei. Representative images were shown (left). (Right) Statistical analysis of the TUNEL and Ki-67. *p < 0.05; **p < 0.01; ***p < 0.001; ****p < 0.0001. Scale bar, 20 μm.

and the apoptosis of tumor cells and growth inhibition of tumor xenograft.[54–58] PLK1 overexpresses in various kinds of tumors, including NKTCL.[17,59–62] We draw the same conclusion from the analyses of GEO database GSE63548, GSE25297, GSE36172, and GSE19067. Clinical studies proved the positive responses of relapsed or refractory non-Hodgkin lymphoma to a PLK1 inhibitor BI 2536. However, the hematologic toxicity like grade 4 thrombocytopenia and neutropenia limited its application in patients.[63] Previous studies found that PLK1 could induce the nuclear exclusion of the FOXO family and negatively regulated their transcriptional activity.[24,64] The FOXO family is a primary tumor suppressor, which is involved in DDR pathway.[25,42] The inactivation of FOXO family is prevailing in many cancers. Specifically, the silence of FOXO3 is frequent in NKTCL owing to 6q21 deletion.[65] FOXO3a promotes DNA repair under low-stress conditions while inducing cell death under a higher level of stress through binding to the promoter of Gadd45.[66] Previous studies found that FOXO3a could activate ATM by increasing its expression and phosphorylation.[25,67] In the current study, we found that ICT inhibited PLK1 to activate FOXO3a and further activate ATM. Our ongoing work found that, as a transcription factor, FOXO3a was predicted by a bioinformatics database to bind to the promoter of ATM to increase its expression (data not shown). Exploring how FOXO3a regulates ATM in NKTCL is our future work.

ICT is competent as a chemosensitizer to achieve lower toxicity and higher efficacy. The current cancer therapies mainly work by inducing DNA damage, at the same time, however, potentially exacerbating pro-tumorigenic genomic instability and enabling the development of resistance.[68] Also, severe side effects often result in intolerance in patients, causing treatment failure. NKTCL patients response poorly to anthracycline-containing therapy owing to the expression of P-glycoprotein.[69] Asparaginase-based therapy may improve the outcome. Asparaginase works by targeting metabolic reprogramming in tumor cells.[70] It depletes an amino acid that is essential for tumor cells but non-essential for normal cells.[70] However, its application indication and dosage are strictly limited owing to the hepatotoxicity and pancreas toxicity, including diabetes mellitus or pancreatitis, hypertriglyceridemia, and coagulation disorders with bleeding or thrombosis.[71] These side effects are mainly caused by the impaired protein synthesis and the interfered L-glutamine metabolism in normal cells.[71] Meanwhile, resistance and relapse frequently occur, leading to dismal outcomes. Recent studies found that asparaginase induced the generation of reactive oxygen species (ROS) and mitochondrial damage, which further enhanced its antitumor activity.[72] Our ongoing work found that ICT also increased the ROS level in NKTCL cells (data not shown). ICT may facilitate the antitumor efficacy of an asparaginase-based regime by jointly increasing ROS level.

As a natural TCM monomer, ICT exerts potent antitumor effects on various tumors by inducing apoptosis, autophagy, or necrosis, while exhibiting minimal toxic side effects in normal cells and mice.[73] Studies have been focusing on the clinical application value of ICT. A clinical trial of ICT treating hepatocellular carcinoma (HCC) revealed its safety and preliminary durable survival benefits.[74] Furthermore, ICT and doxorubicin played a synergistic role in treating HCC.[75] The nanotechnology-mediated co-delivery of ICT and doxorubicin further increased the treatment efficacy *in vivo*.[75] Our further goal is to find a proper nanoparticle formulation to deliver ICT and GELOX.

In summary, our work demonstrated the effects and mechanism of ICT inhibiting NKTCL. We propose it as a potential chemotherapeutic drug and safe chemosensitizer to facilitate clinical NKTCL treatment.

MATERIALS AND METHODS

Cell culture

Three NKTCL cell lines—SNT-8, SNK-10, and SNT-16 (kind gifts from Dr. Norio Shimizu at Tokyo Medical and Dental University)—were cultured in RPMI-1640 medium (Hyclone) supplemented with 10% human plasma (Gemini) and 700 U/mL recombinant human interleukin-2 (PeproTech). The NK-92 MI cell line was purchased from ATCC (CRL-2408) and cultured in Alpha Minimum Essential medium without ribonucleosides and deoxyribonucleosides (Gibco) but with 2 mM L-glutamine and 1.5 g/L sodium bicarbonate (Life Technologies) supplemented with 12.5% fetal bovine serum (Biological Industries), 12.5% horse serum (Biological Industries), 0.2 mM inositol (Solarbio), 0.1 mM 2-mercaptoethanol (Solarbio) and 0.02 mM folic acid (Sigma Aldrich). All cells were cultivated at 37°C in a humidified atmosphere of 5% CO_2 in the air.

Cell proliferation assay

Cells were cultured in complete medium containing dimethyl sulfoxide (DMSO, as control), ICT (Winherb Medical Science), or BI 2536 (Beyotime) at the indicated concentrations for the indicated time. Cell viability was measured by Cell Counting Kit-8 (CCK-8, Beyotime) following the manufacturer's protocol. The absorbance at 450 nm was measured using an ELX808 microplate spectrophotometer (BioTek Instruments). The cell viability ratio was calculated as:

$$\text{Cell viability rate} = (\text{average OD of ICT or / and BI 2536 treated wells} - \text{average OD of blank wells}) / (\text{average OD of control wells} - \text{average OD of blank wells}) \times 100\%$$

Each experiment was carried out in six replicates and results were calculated over three independent experiments.

Apoptosis detection

Cells were double-labeled with Annexin V-FITC and PI using FITC Annexin V Apoptosis Detection Kit (BD) according to the manufacturer's instructions and were examined by flow cytometer FACS Calibur (BD). The data were analyzed by FlowJo software.

Gene expression profiles of ICT treated NKTCL cells and GEO datamining

Gene expression profiles of three NKTCL cell lines treated with ICT or DMSO for 12 h were measured using RNA-seq. Three replicates per group were performed. Enriched and purified mRNA was fragmented and reverse transcribed to double-strand cDNA by N6 random primer, on which "A" stickiness and "T" adaptor were added at the 3′ end. The cDNA library was created by PCR and sequenced on BGISEQ-500 Instrument (BGI). Quality control of raw data was performed by data filtering and reads mapping. For gene expression estimation, clean reads were aligned to reference gene and genome using Bowtie2 and HISAT, respectively. The DEGs were screened based on the NOIseq package method. DEGs were selected with a fold change by two or more fold and a p value of less than 0.05. GO and KEGG pathway analyses were performed using DAVID (https://david.ncifcrf.gov/). The PPI network was constructed using the Search Tool for the Retrieval of Interacting Genes database and was drawn by Cytoscape (version 3.7.1). The interaction with a combined score of more than 0.4 was considered statistically significant. The core modules in the PPI networks were identified using MCODE, a plug-in of Cytoscape.

The GSE63548, GSE25297, GSE36172, and GSE19067 datasets were downloaded from the GEO database (https://www.ncbi.nlm.nih.gov/geo/) and the expressions of PLK1 in normal lymph nodes and NKTCL cell lines were extracted.

DSS crosslinking and western blot

To detect the Chk2 dimer, DSS (disuccinimidyl suberate, Pierce) crosslinking was performed. DSS is a homobifunctional N-hydroxysuccinimide ester that reacts with primary amino groups (-NH2) to form stable amide bonds. DSS was dissolved in DMSO immediately before use. A final concentration of 1 mM DSS was added into cell suspension in PBS. The crosslinking proceeded for 30 min at room temperature before cell lysis.

Cells or tumor tissues were lysed by RIPA supplemented with Phos-stop (Roche) and PMSF (Beyotime). Total lysates were quantified by BCA Protein Assay Kit (Beyotime). Equal amounts of proteins were separated by 4%–12% or 4%–20% PAGE using tris-mops electrophoresis buffer (GenScript), and were transferred onto PVDF membranes (Merck Millipore). Specific primary antibodies were as follows: PLK1 (#4513, CST); p-PLK1 (ab155095, Abcam); Chk2 (#6334, CST); p-Chk2 T68 (#2197, CST); p-Chk2 T387 (ab55319, Abcam); p53 (ab1101, Abcam); p-p53 (ab76242, Abcam); ATM (ab26350, Abcam); p-ATM (ab81292, Abcam); FOXO3a (#12829, CST); γH2Ax (Ab26350, Abcam); GAPDH (#5174, CST); β-Actin (#4967, CST); and α-tublin (#2144, CST). The intensities of the protein bands were quantified using grayscale scanner ImageJ (version 1.52i).

IHC, IF staining, and TUNEL assay

Tissues were fixed in 4% formaldehyde and embedded in paraffin. The following primary antibodies were used for IHC staining at the indicated dilution: PLK1 (1:50, #4513, CST), p-p53 (1:200, ab76242, Abcam), p-Chk2 T68 (1:200, #2197, CST), Ki-67 (1:600, GB111499, Servicebio). The smears were scanned using Panoramic MIDI (3DHISTECH) and scored by two pathologists following the double-blind principle.

IF staining was performed as described previously.[76] The primary antibodies were against FOXO3a (1:400; #12829, CST; 66,428-1, Proteintech) and PLK1 (#4513, CST). Alexa Fluor 555-labeled donkey anti-rabbit IgG and FITC-labeled goat anti-mouse IgG (Beyotime) were used. Cell nuclei were stained with DAPI (Beyotime).

Fragmented DNA *in situ* labeling was performed with the One Step TUNEL Apoptosis Assay Kit (Beyotime). The DNA fragments were labeled with fluorescein-dideoxy-UTP by the TUNEL and the nuclei were counterstained with DAPI (Beyotime). The percentage of TUNEL-positive cells (apoptotic cells) was evaluated.

RNA extraction and quantitative PCR

Total RNA isolation, reverse transcription, and quantitative PCR was performed as previously described.[17] Primers for PLK1 and β-actin (a loading control) were as before.[17]

Co-IP

The Co-IP assay was performed using a Co-IP Kit (ThermoFisher Scientific) following the manufacturer's protocol. Cell lysates were incubated with specific antibodies or IgG and rotate for 2 h. Then protein A/G magnetic beads were added. After rotating for 1.5 h, the proteins on the beads were eluted by low PH buffer.

Lentivirus transfection of NK-92 MI cell line

The NK-92 MI cell line was transfected with lentivirus (Hanbio Biotechnology) to attain stable tet on PLK1 or EV expression. Puromycin (Beyotime) was used to select (2 μg/mL) and sustain (1 μg/mL) the stably transfected cells.

Xenograft model establishment and *in vivo* antitumor treatment assay

Animal experiments were approved by the experimental animal ethics committee of Fudan University. NK-92 MI cells were stably transfected with luciferase gene and named NK-92 MI Luc. NK-92 MI or NK-92 MI Luc cells were mixed with high concentration Matrigel (Corning) and injected subcutaneously into the right flank regions of 8-week-old female NOG mice (Vital River Laboratory Animal Technology), 5×10^6 cells per mouse. When the tumor volume reached 300 mm^3, the mice were randomized into different groups and treated at the indicated days with vehicle, or ICT and/or GELOX regimen. ICT, gemcitabine (CSN Pharm), and oxaliplatin (CSN Pharm) were prepared in 5% DMSO and 40% polyethylene glycol 400 (CSNpharm), 5% Tween-80 (CSNpharm), and 50% PBS. L-asparaginase (Sigma) was prepared in PBS. The tumor length and width and mice weight were measured every other day. The tumor volume (mm^3) was calculated using the following formula: $V = 0.52 \times \text{length} \times \text{width}^2$. Bioluminescence imaging was performed using IVIS (PerkinElmer) imaging system. Live animal images were acquired 10 min after intraperitoneal injection of D-Luciferin (3 mg/mouse; Beyotime). The mice were euthanized and tumor tissues were collected and weighed after treatment finished.

Statistical analyses

Statistical analyses were conducted by one-way ANOVA or the Student *t*-test using GraphPad Prism 8. A p value of less than 0.05 was considered significant.

SUPPLEMENTAL INFORMATION

Supplemental information can be found online at https://doi.org/10.1016/j.omto.2022.04.012.

ACKNOWLEDGMENTS

This study was supported by the National Natural Science Foundation of China (Grant No. 81470352 and 81770208).

AUTHOR CONTRIBUTIONS

S.W. and X. W. designed the research, C. Z., H. X., X. S., and L. C. performed research and analyzed data, S. W., X. W., and B. C. supervised the research. C. Z. and H. L. wrote the paper.

DECLARATION OF INTERESTS

The authors declare no competing interests.

REFERENCES

1. Swerdlow, S.H.C.E., Harris, N.L., Jaffe, E.S., Pileri, S.A., Stein, H., and Thiele, J. (2017). WHO Classification of Tumours of Haematopoietic and Lymphoid Tissues, Revised, Fourth edition (IARC).
2. Yamaguchi, M., Suzuki, R., and Oguchi, M. (2018). Advances in the treatment of extranodal NK/T-cell lymphoma, nasal type. Blood *131*, 2528–2540. https://doi.org/10.1182/blood-2017-12-791418.
3. Yamaguchi, M., and Miyazaki, K. (2017). Current treatment approaches for NK/T-cell lymphoma. J. Clin. Exp. Hematopathol. *57*, 98–108. https://doi.org/10.3960/jslrt.17018.
4. Kwong, Y.L., Kim, W.S., Lim, S.T., Kim, S.J., Tang, T., Tse, E., Leung, A.Y.H., and Chim, C.S. (2012). SMILE for natural killer/T-cell lymphoma: analysis of safety and efficacy from the Asia Lymphoma Study Group. Blood *120*, 2973–2980. https://doi.org/10.1182/blood-2012-05-431460.
5. Yamaguchi, M., Kwong, Y.L., Kim, W.S., Maeda, Y., Hashimoto, C., Suh, C., Izutsu, K., Ishida, F., Isobe, Y., Sueoka, E., et al. (2011). Phase II study of SMILE chemotherapy for newly diagnosed stage IV, relapsed, or refractory extranodal natural killer (NK)/T-cell lymphoma, nasal type: the NK-Cell Tumor Study Group Study. J. Clin. Oncol. *29*, 4410–4416. https://doi.org/10.1200/jco.2011.35.6287.
6. Bi, X.W., Xia, Y., Zhang, W.W., Sun, P., Liu, P.P., Wang, Y., Huang, J.J., Jiang, W.Q., and Li, Z.M. (2015). Radiotherapy and PGEMOX/GELOX regimen improved prognosis in elderly patients with early-stage extranodal NK/T-cell lymphoma. Ann. Hematol. *94*, 1525–1533. https://doi.org/10.1007/s00277-015-2395-y.
7. de Mel, S., Tan, J.Z.C., Jeyasekharan, A.D., Chng, W.J., and Ng, S.B. (2019). Transcriptomic abnormalities in Epstein Barr virus associated T/NK lymphoproliferative disorders. Front. Pediatr. *6*, 405. https://doi.org/10.3389/fped.2018.00405.
8. Ahn, J.Y., Li, X., Davis, H.L., and Canman, C.E. (2002). Phosphorylation of threonine 68 promotes oligomerization and autophosphorylation of the Chk2 protein kinase via the forkhead-associated domain. J. Biol. Chem. *277*, 19389–19395. https://doi.org/10.1074/jbc.m200822200.
9. Schwarz, J.K., Lovly, C.M., and Piwnica-Worms, H. (2003). Regulation of the Chk2 protein kinase by oligomerization-mediated cis- and trans-phosphorylation. Mol. Cancer Res. *1*, 598–609.
10. Chen, L., Gilkes, D.M., Pan, Y., Lane, W.S., and Chen, J. (2005). ATM and Chk2-dependent phosphorylation of MDMX contribute to p53 activation after DNA damage. EMBO J. *24*, 3411–3422. https://doi.org/10.1038/sj.emboj.7600812.
11. Jackson, S.P., and Bartek, J. (2009). The DNA-damage response in human biology and disease. Nature *461*, 1071–1078. https://doi.org/10.1038/nature08467.
12. Zhang, X.P., Liu, F., Cheng, Z., and Wang, W. (2009). Cell fate decision mediated by p53 pulses. Proc. Natl. Acad. Sci. U S A *106*, 12245–12250. https://doi.org/10.1073/pnas.0813088106.
13. Bartek, J., Bartkova, J., and Lukas, J. (2007). DNA damage signalling guards against activated oncogenes and tumour progression. Oncogene *26*, 7773–7779. https://doi.org/10.1038/sj.onc.1210881.
14. Roos, W.P., and Kaina, B. (2006). DNA damage-induced cell death by apoptosis. Trends Mol. Med. *12*, 440–450. https://doi.org/10.1016/j.molmed.2006.07.007.
15. Vogelstein, B., Papadopoulos, N., Velculescu, V.E., Zhou, S., Diaz, L.A., Jr., and Kinzler, K.W. (2013). Cancer genome landscapes. Science *339*, 1546–1558. https://doi.org/10.1126/science.1235122.
16. Weinstein, J.N., Collisson, E.A., Mills, G.B., Shaw, K.R., Stuart, J.M., Shmulevich, I., Ellrott, K., Ozenberger, B.A., Ellrott, K., Shmulevich, I., et al. (2013). The cancer genome atlas pan-cancer analysis project. Nat. Genet. *45*, 1113–1120. https://doi.org/10.1038/ng.2764.
17. Sui, X., Zhang, C., Jiang, Y., Zhou, J., Xu, C., Tang, F., Chen, B., Xu, H., Wang, S., and Wang, X. (2020). Resveratrol activates DNA damage response through inhibition of polo-like kinase 1 (PLK1) in natural killer/T cell lymphoma. Ann. Transl. Med. *8*, 688. https://doi.org/10.21037/atm-19-4324.
18. Hyun, S.Y., Hwan, H.I., and Jang, Y.J. (2014). Polo-like kinase-1 in DNA damage response. BMB Rep. *47*, 249–255. https://doi.org/10.5483/bmbrep.2014.47.5.061.
19. Golsteyn, R.M., Mundt, K.E., Fry, A.M., and Nigg, E.A. (1995). Cell cycle regulation of the activity and subcellular localization of Plk1, a human protein kinase implicated in mitotic spindle function. J. Cell Biol. *129*, 1617–1628. https://doi.org/10.1083/jcb.129.6.1617.
20. van Vugt, M.A.T.M., and Medema, R.H. (2005). Getting in and out of mitosis with Polo-like kinase-1. Oncogene *24*, 2844–2859. https://doi.org/10.1038/sj.onc.1208617.
21. Benada, J., Burdová, K., Lidak, T., von Morgen, P., and Macurek, L. (2015). Polo-like kinase 1 inhibits DNA damage response during mitosis. Cell Cycle *14*, 219–231. https://doi.org/10.4161/15384101.2014.977067.
22. Zannini, L., Delia, D., and Buscemi, G. (2014). CHK2 kinase in the DNA damage response and beyond. J. Mol. Cell Biol. *6*, 442–457. https://doi.org/10.1093/jmcb/mju045.
23. Ando, K., Ozaki, T., Yamamoto, H., Furuya, K., Hosoda, M., Hayashi, S., Fukuzawa, M., and Nakagawara, A. (2004). Polo-like kinase 1 (Plk1) inhibits p53 function by physical interaction and phosphorylation. J. Biol. Chem. *279*, 25549–25561. https://doi.org/10.1074/jbc.m314182200.
24. Bucur, O., Stancu, A.L., Muraru, M.S., Melet, A., Petrescu, S.M., and Khosravi-Far, R. (2014). PLK1 is a binding partner and a negative regulator of FOXO3 tumor suppressor. Discoveries (Craiova) *2*, e16. https://doi.org/10.15190/d.2014.8.
25. Tsai, W.B., Chung, Y.M., Takahashi, Y., Xu, Z., and Hu, M.C.T. (2008). Functional interaction between FOXO3a and ATM regulates DNA damage response. Nat. Cell Biol. *10*, 460–467. https://doi.org/10.1038/ncb1709.
26. Wang, X., Feng, Y., Wang, N., Cheung, F., Tan, H.Y., Zhong, S., Li, C., and Kobayashi, S. (2014). Chinese medicines induce cell death: the molecular and cellular mechanisms for cancer therapy. Biomed. Res. Int. *2014*, 1–14. https://doi.org/10.1155/2014/530342.
27. Wang, Z., Zhang, X., Wang, H., Qi, L., and Lou, Y. (2007). Neuroprotective effects of icaritin against beta amyloid-induced neurotoxicity in primary cultured rat neuronal cells via estrogen-dependent pathway. Neuroscience *145*, 911–922. https://doi.org/10.1016/j.neuroscience.2006.12.059.
28. Jiang, M.C., Chen, X.H., Zhao, X., Zhang, X.J., and Chen, W.F. (2016). Involvement of IGF-1 receptor signaling pathway in the neuroprotective effects of Icaritin against MPP(+)-induced toxicity in MES23.5 cells. Eur. J. Pharmacol. *786*, 53–59. https://doi.org/10.1016/j.ejphar.2016.05.031.
29. Huang, J., Yuan, L., Wang, X., Zhang, T.L., and Wang, K. (2007). Icaritin and its glycosides enhance osteoblastic, but suppress osteoclastic, differentiation and activity in vitro. Life Sci. *81*, 832–840. https://doi.org/10.1016/j.lfs.2007.07.015.
30. Wo, Y.B., Zhu, D.Y., Hu, Y., Wang, Z.Q., Liu, J., and Lou, Y.J. (2008). Reactive oxygen species involved in prenylflavonoids, icariin and icaritin, initiating cardiac differentiation of mouse embryonic stem cells. J. Cell. Biochem. *103*, 1536–1550. https://doi.org/10.1002/jcb.21541.
31. Hu, J., Yang, T., Xu, H., Hu, M., Wen, H., and Jiang, H. (2016). A novel anticancer agent icaritin inhibited proinflammatory cytokines in TRAMP mice. Int. Urol. Nephrol. *48*, 1649–1655. https://doi.org/10.1007/s11255-016-1341-9.
32. Zhu, J.F., Li, Z.J., Zhang, G.S., Meng, K., Kuang, W.Y., Li, J., Zhou, X.F., Li, R.J., Peng, H.L., Dai, C.W., et al. (2011). Icaritin shows potent anti-leukemia activity on chronic myeloid leukemia in vitro and in vivo by regulating MAPK/ERK/JNK and JAK2/STAT3/AKT signalings. PLoS One *6*, e23720. https://doi.org/10.1371/journal.pone.0023720.
33. Zheng, Q., Liu, W.W., Li, B., Chen, H.J., Zhu, W.S., Yang, G.X., Chen, M.J., and He, G.Y. (2014). Anticancer effect of icaritin on human lung cancer cells through inducing S phase cell cycle arrest and apoptosis. J. Huazhong Univ. Sci. Technol. Med. Sci. *34*, 497–503. https://doi.org/10.1007/s11596-014-1305-1.
34. Sun, L., Peng, Q., Qu, L., Gong, L., and Si, J. (2015). Anticancer agent icaritin induces apoptosis through caspase-dependent pathways in human hepatocellular carcinoma cells. Mol. Med. Rep. *11*, 3094–3100. https://doi.org/10.3892/mmr.2014.3007.
35. Guo, Y., Zhang, X., Meng, J., and Wang, Z.Y. (2011). An anticancer agent icaritin induces sustained activation of the extracellular signal-regulated kinase (ERK) pathway and inhibits growth of breast cancer cells. Eur. J. Pharmacol. *658*, 114–122. https://doi.org/10.1016/j.ejphar.2011.02.005.
36. Li, C., Peng, W., Song, X., Wang, Q., and Wang, W. (2016). Anticancer effect of icaritin inhibits cell growth of colon cancer through reactive oxygen species, Bcl-2 and

cyclin D1/E signaling. Oncol. Lett. *12*, 3537–3542. https://doi.org/10.3892/ol.2016.5089.

37. Zhou, C., Chen, Z., Lu, X., Wu, H., Yang, Q., and Xu, D. (2016). Icaritin activates JNK-dependent mPTP necrosis pathway in colorectal cancer cells. Tumour Biol. *37*, 3135–3144. https://doi.org/10.1007/s13277-015-4134-3.

38. Pan, X.W., Li, L., Huang, Y., Huang, H., Xu, D.F., Gao, Y., Chen, L., Ren, J.Z., Cao, J.W., Hong, Y., et al. (2016). Icaritin acts synergistically with epirubicin to suppress bladder cancer growth through inhibition of autophagy. Oncol. Rep. *35*, 334–342. https://doi.org/10.3892/or.2015.4335.

39. Tong, J.S., Zhang, Q.H., Huang, X., Fu, X.Q., Qi, S.T., Wang, Y.P., Hou, Y., Sheng, J., and Sun, Q.Y. (2011). Icaritin causes sustained ERK1/2 activation and induces apoptosis in human endometrial cancer cells. PLoS One *6*, e16781. https://doi.org/10.1371/journal.pone.0016781.

40. Li, Q., Huai, L., Zhang, C., Wang, C., Jia, Y., Chen, Y., Yu, P., Wang, H., Rao, Q., Wang, M., et al. (2013). Icaritin induces AML cell apoptosis via the MAPK/ERK and PI3K/AKT signal pathways. Int. J. Hematol. *97*, 617–623. https://doi.org/10.1007/s12185-013-1317-9.

41. van Vugt, M.A.T.M., Gardino, A.K., Linding, R., Ostheimer, G.J., Reinhardt, H.C., Ong, S.E., Tan, C.S., Miao, H., Keezer, S.M., Li, J., et al. (2010). A mitotic phosphorylation feedback network connects Cdk1, Plk1, 53BP1, and Chk2 to inactivate the G(2)/M DNA damage checkpoint. PLoS Biol. *8*, e1000287. https://doi.org/10.1371/journal.pbio.1000287.

42. Chung, Y.M., Park, S.H., Tsai, W.B., Wang, S.Y., Ikeda, M.A., Berek, J.S., Chen, D.J., and Hu, M.C.T. (2012). FOXO3 signalling links ATM to the p53 apoptotic pathway following DNA damage. Nat. Commun. *3*, 1000. https://doi.org/10.1038/ncomms2008.

43. Fasano, C., Disciglio, V., Bertora, S., Lepore Signorile, M., and Simone, C. (2019). FOXO3a from the nucleus to the mitochondria: a round trip in cellular stress response. Cells *8*, 1110. https://doi.org/10.3390/cells8091110.

44. Zhang, Y., Lou, Y., Wang, J., Yu, C., and Shen, W. (2021). Research status and molecular mechanism of the traditional Chinese medicine and antitumor therapy combined strategy based on tumor microenvironment. Front. Immunol. *11*, 609705. https://doi.org/10.3389/fimmu.2020.609705.

45. Wu, T., Wang, S., Wu, J., Lin, Z., Sui, X., Xu, X., Shimizu, N., Chen, B., and Wang, X. (2015). Icaritin induces lytic cytotoxicity in extranodal NK/T-cell lymphoma. J. Exp. Clin. Cancer Res. *34*, 17. https://doi.org/10.1186/s13046-015-0133-x.

46. Lindahl, T., and Barnes, D.E. (2000). Repair of endogenous DNA damage. Cold Spring Harb. Symp. Quant. Biol. *65*, 127–134. https://doi.org/10.1101/sqb.2000.65.127.

47. Reuvers, T.G.A., Kanaar, R., and Nonnekens, J. (2020). DNA damage-inducing anticancer therapies: from global to precision damage. Cancers *12*, 2098. https://doi.org/10.3390/cancers12082098.

48. Zhou, C., Lin, A., Cao, M., Ding, W., Mou, W., Guo, N., Chen, Z., Zhang, J., and Luo, P. (2021). Activation of the DDR pathway leads to the down-regulation of the TGFβ pathway and a better response to ICIs in patients with metastatic urothelial carcinoma. Front. Immunol. *12*, 634741. https://doi.org/10.3389/fimmu.2021.634741.

49. Xiong, J., Cui, B.W., Wang, N., Dai, Y.T., Zhang, H., Wang, C.F., Zhong, H.J., Cheng, S., Ou-Yang, B.S., Hu, Y., et al. (2020). Genomic and transcriptomic characterization of natural killer T cell lymphoma. Cancer Cell *37*, 403–419.e6.

50. O'Connor, M. (2015). Targeting the DNA damage response in cancer. Mol. Cell *60*, 547–560. https://doi.org/10.1016/j.molcel.2015.10.040.

51. Cheng, B., Pan, W., Xing, Y., Xiao, Y., Chen, J., and Xu, Z. (2022). Recent advances in DDR (DNA damage response) inhibitors for cancer therapy. Eur. J. Med. Chem. *230*, 114109. https://doi.org/10.1016/j.ejmech.2022.114109.

52. Bryant, H.E., Schultz, N., Thomas, H.D., Parker, K.M., Flower, D., Lopez, E., Kyle, S., Meuth, M., Curtin, N.J., and Helleday, T. (2005). Specific killing of BRCA2-deficient tumours with inhibitors of poly(ADP-ribose) polymerase. Nature *434*, 913–917. https://doi.org/10.1038/nature03443.

53. Farmer, H., McCabe, N., Lord, C.J., Tutt, A.N., Johnson, D.A., Richardson, T.B., Santarosa, M., Dillon, K.J., Hickson, I., Knights, C., et al. (2005). Targeting the DNA repair defect in BRCA mutant cells as a therapeutic strategy. Nature *434*, 917–921. https://doi.org/10.1038/nature03445.

54. Steegmaier, M., Hoffmann, M., Baum, A., Lenart, P., Petronczki, M., Krssak, M., Gurtler, U., Garin-Chesa, P., Lieb, S., Quant, J., et al. (2007). BI 2536, a potent and selective inhibitor of polo-like kinase 1, inhibits tumor growth in vivo. Curr. Biol. *17*, 316–322. https://doi.org/10.1016/j.cub.2006.12.037.

55. Reagan-Shaw, S., and Ahmad, N. (2005). Silencing of polo-like kinase (Plk) 1 via siRNA causes induction of apoptosis and impairment of mitosis machinery in human prostate cancer cells: implications for the treatment of prostate cancer. FASEB J. *19*, 611–614. https://doi.org/10.1096/fj.04-2910fje.

56. Nogawa, M., Yuasa, T., Kimura, S., Tanaka, M., Kuroda, J., Sato, K., Yokota, A., Segawa, H., Toda, Y., Kageyama, S., et al. (2005). Intravesical administration of small interfering RNA targeting PLK-1 successfully prevents the growth of bladder cancer. J. Clin. Invest. *115*, 978–985. https://doi.org/10.1172/jci23043.

57. Wang, Y., Wu, L., Yao, Y., Lu, G., Xu, L., and Zhou, J. (2018). Polo-like kinase 1 inhibitor BI 6727 induces DNA damage and exerts strong antitumor activity in small cell lung cancer. Cancer Lett. *436*, 1–9. https://doi.org/10.1016/j.canlet.2018.08.007.

58. Liu, X., Lei, M., and Erikson, R.L. (2006). Normal cells, but not cancer cells, survive severe Plk1 depletion. Mol. Cell. Biol. *26*, 2093–2108. https://doi.org/10.1128/mcb.26.6.2093-2108.2006.

59. Ng, S.B., Selvarajan, V., Huang, G., Zhou, J., Feldman, A.L., Law, M., Kwong, Y.L., Shimizu, N., Kagami, Y., Aozasa, K., et al. (2011). Activated oncogenic pathways and therapeutic targets in extranodal nasal-type NK/T cell lymphoma revealed by gene expression profiling. J. Pathol. *223*, 496–510. https://doi.org/10.1002/path.2823.

60. Takahashi, T., Sano, B., Nagata, T., Kato, H., Sugiyama, Y., Kunieda, K., Kimura, M., Okano, Y., and Saji, S. (2003). Polo-like kinase 1 (PLK1) is overexpressed in primary colorectal cancers. Cancer Sci. *94*, 148–152. https://doi.org/10.1111/j.1349-7006.2003.tb01411.x.

61. Takai, N., Miyazaki, T., Fujisawa, K., Nasu, K., Hamanaka, R., and Miyakawa, I. (2001). Polo-like kinase (PLK) expression in endometrial carcinoma. Cancer Lett. *169*, 41–49. https://doi.org/10.1016/s0304-3835(01)00522-5.

62. Knecht, R., Elez, R., Oechler, M., Solbach, C., von Ilberg, C., and Strebhardt, K. (1999). Prognostic significance of polo-like kinase (PLK) expression in squamous cell carcinomas of the head and neck. Cancer Res. *59*, 2794–2797.

63. Vose, J.M., Friedberg, J.W., Waller, E.K., Cheson, B.D., Juvvigunta, V., Fritsch, H., Petit, C., Munzert, G., and Younes, A. (2013). The Plk1 inhibitor BI 2536 in patients with refractory or relapsed non-Hodgkin lymphoma: a phase I, open-label, single dose-escalation study. Leuk. Lymphoma *54*, 708–713. https://doi.org/10.3109/10428194.2012.729833.

64. Gheghiani, L., Shang, S., and Fu, Z. (2020). Targeting the PLK1-FOXO1 pathway as a novel therapeutic approach for treating advanced prostate cancer. Sci. Rep. *10*, 12327. https://doi.org/10.1038/s41598-020-69338-8.

65. Huang, Y., de Reynies, A., de Leval, L., Ghazi, B., Martin-Garcia, N., Travert, M., Bosq, J., Briere, J., Petit, B., Thomas, E., et al. (2010). Gene expression profiling identifies emerging oncogenic pathways operating in extranodal NK/T-cell lymphoma, nasal type. Blood *115*, 1226–1237. https://doi.org/10.1182/blood-2009-05-221275.

66. Tran, H., Brunet, A., Grenier, J.M., Datta, S.R., Fornace, A.J., Jr., DiStefano, P.S., Chiang, L.W., and Greenberg, M.E. (2002). DNA repair pathway stimulated by the forkhead transcription factor FOXO3a through the Gadd45 protein. Science *296*, 530–534. https://doi.org/10.1126/science.1068712.

67. Yalcin, S., Zhang, X., Luciano, J.P., Mungamuri, S.K., Marinkovic, D., Vercherat, C., Sarkar, A., Grisotto, M., Taneja, R., and Ghaffari, S. (2008). Foxo3 is essential for the regulation of ataxia telangiectasia mutated and oxidative stress-mediated homeostasis of hematopoietic stem cells. J. Biol. Chem. *283*, 25692–25705. https://doi.org/10.1074/jbc.m800517200.

68. Khanna, A. (2015). DNA damage in cancer therapeutics: a boon or a curse? Cancer Res. *75*, 2133–2138. https://doi.org/10.1158/0008-5472.can-14-3247.

69. Tse, E., and Kwong, Y.L. (2019). NK/T-cell lymphomas. Best Pract. Res. Clin. Haematol. *32*, 253–261. https://doi.org/10.1016/j.beha.2019.06.005.

70. Obama, K., Tara, M., and Niina, K. (2003). L-asparaginase-based induction therapy for advanced extranodal NK/T-cell lymphoma. Int. J. Hematol. *78*, 248–250. https://doi.org/10.1007/bf02983802.

71. Lanvers-Kaminsky, C. (2017). Asparaginase pharmacology: challenges still to be faced. Cancer Chemother. Pharmacol. *79*, 439–450. https://doi.org/10.1007/s00280-016-3236-y.

72. Soncini, D., Minetto, P., Martinuzzi, C., Becherini, P., Fenu, V., Guolo, F., Todoerti, K., Calice, G., Contini, P., Miglino, M., et al. (2020). Amino acid depletion triggered by L-asparaginase sensitizes MM cells to carfilzomib by inducing mitochondria ROS-mediated cell death. Blood Adv. *4*, 4312–4326. https://doi.org/10.1182/bloodadvances.2020001639.

73. Zhang, C., Sui, X., Jiang, Y., Wang, X., and Wang, S. (2020). Antitumor effects of icaritin and the molecular mechanisms. Discov. Med. *29*, 5–16.

74. Fan, Y., Li, S., Ding, X., Yue, J., Jiang, J., Zhao, H., Hao, R., Qiu, W., Liu, K., Li, Y., et al. (2019). First-in-class immune-modulating small molecule Icaritin in advanced hepatocellular carcinoma: preliminary results of safety, durable survival and immune biomarkers. BMC Cancer *19*, 279. https://doi.org/10.1186/s12885-019-5471-1.

75. Yu, Z., Guo, J., Hu, M., Gao, Y., and Huang, L. (2020). Icaritin exacerbates mitophagy and synergizes with doxorubicin to induce immunogenic cell death in hepatocellular carcinoma. ACS Nano *14*, 4816–4828. https://doi.org/10.1021/acsnano.0c00708.

76. Sui, X., Zhang, C., Zhou, J., Cao, S., Xu, C., Tang, F., Zhi, X., Chen, B., Wang, S., and Yin, L. (2017). Resveratrol inhibits Extranodal NK/T cell lymphoma through activation of DNA damage response pathway. J. Exp. Clin. Cancer Res. *36*, 133. https://doi.org/10.1186/s13046-017-0601-6.